Phase Transitions, 1995, Vol. 54, pp. 123–129
Reprints available directly from the publisher
Photocopying permitted by license only

THE STRUCTURAL PHASE TRANSITION IN $BaTiO_3$ IN A STATIC ELECTRIC FIELD

Y. SOEJIMA, T. NINOMIYA and H. YAMADA

Department of Physics, Kyushu University, Fukuoka 812–81, Japan

(Received 10 May 1995)

The effect of an external electric field on the diffraction profile of cubic $BaTiO_3$ has been examined by high-resolution X-ray diffraction. Two remarkable changes in the 400 diffraction profiles are observed: one is a peak narrowing due to a rearrangement of grains at temperature 10–20 K above Curie temperature, and the other is a peak broadening and collapsing observed on a single grain at temperatures closer to the transition. It is also found that no second phase appears in the crystal in the temperature range related to the observations mentioned above. The results indicate that a kind of ferroelectricity can be induced by an external field even in the cubic structure.

KEY WORDS: $BaTiO_3$, cubic phase, high-resolution X-ray diffraction, external-field

1 INTRODUCTION

Although the cubic-to-tetragonal phase transition in $BaTiO_3$ has been explained as an example of the displacive type, some features are consistent with an order-disorder transition: proposed models of disorder in the cubie phase are dynamical domains (Takahashi, 1961), dynamical clusters (Inoue, 1983; Inoue and Akimoto, 1983), random distribution of rods of chain structures (Comes, Lambert and Guinier, 1968) and local disorder of eight sites (Itoh, Zeng, Nakamura and Mishima, 1985; Dougherty, Wiederrecht and Nelson, 1994). In the case of an order-disorder transition, we expect influence from an external electric field on the X-ray diffraction profile even in the cubic phase. In the present paper, we examine a possible change in the diffraction profiles in a variable static electric field.

For high-resolution measurements of the two-dimensional intensity distribution in reciprocal space, 2θ-resolved high-angle double-crystal X-ray diffractometry (2θ-resolved HADOX) has been developed (Soejima, Tomonaga, Onitsuka and Okazaki, 1991), and applied to the study of the transition in $BaTiO_3$ (Tomonaga, Soejima and Okazaki, 1990; Onitsuka, Hatakeyama, Soejima and Okazaki, 1994). It has been found that the method is also suitable for characterization of specimen crystals in high resolution. Since the effect of an external field on the diffraction pattern was expected to be small, if any, the 2θ-resolved HADOX was applied for the present work.

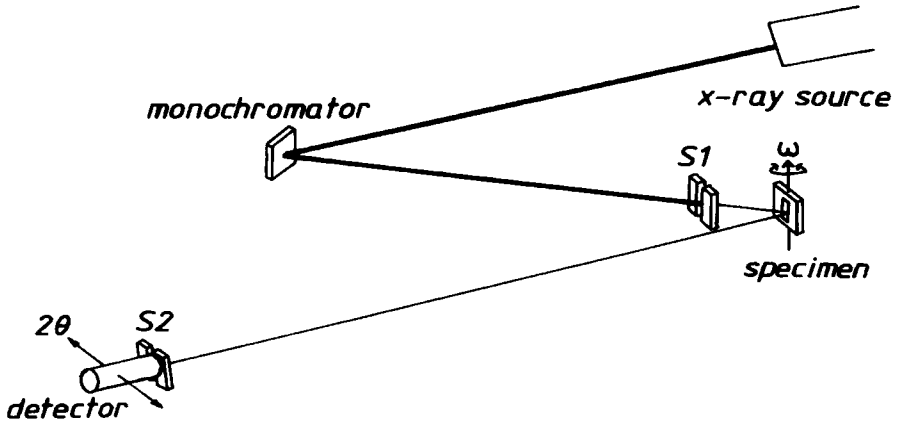

Figure 1 Experimental arrangement of 2θ-resolved HADOX.

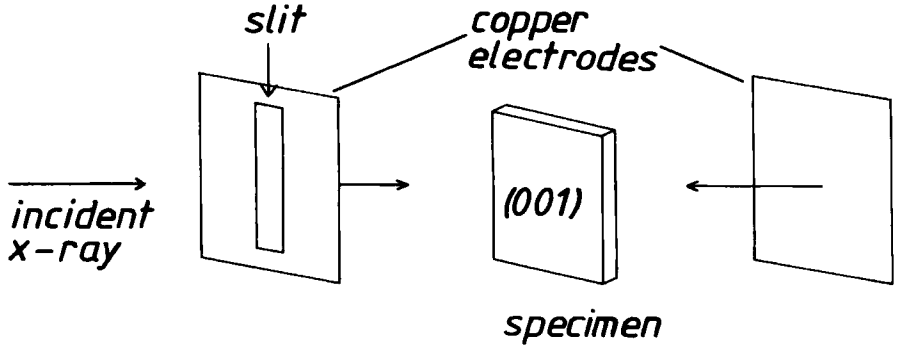

Figure 2 Specimen sandwiched between copper electrodes to apply the electric field in the direction parallel to [001]. A slit 1×5 mm^2 in size is used before the front electrode for incident and diffracted beams.

2 EXPERIMENTAL

The experimental arrangement of the diffractometer is schematically shown in Figure 1; two slits S1 and S2 were introduced into the original version of HADOX (Okazaki and Ohama, 1979; Ohama, Sakashita and Okazaki, 1979) to limit the beam size in the diffractometer plane, and to limit the window size of the scintillation detector, respectively. The sizes of S1 and S2 define the accuracy and resolution of the diffractometer in 2θ (Soejima *et al.*, 1991). The combination of ω and 2θ step scannings makes it possible to determine the two-dimensional intensity distribution on a reciprocal lattice plane parallel to the plane of the diffractometer. By this method, a change in the diffraction profile can be specified in connection with the lattice spacing and the axial orientation. In the present experiment, incident FeKα_1 beams were monochromatized with 400 of $SrTiO_3$ at $\theta \sim 82.5°$. The operating

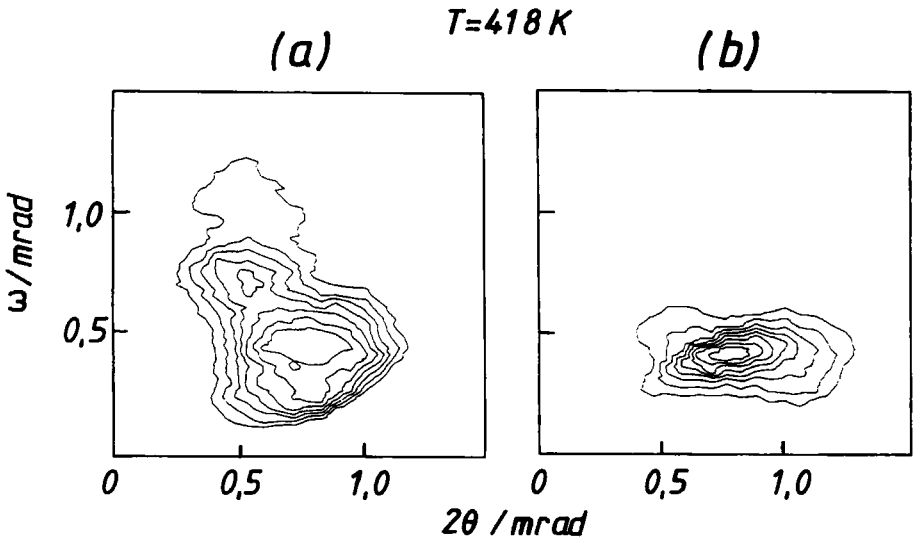

Figure 3 Intensity contour maps of 400 peak at 418 K, 17 K above T_c: (a) in E=0, and (b) in E=0.87 kV/mm.

condition in the fine-focusing mode of a rotating-anode X-ray generator (Rigaku RU-200) was 50 kV and 10 mA. To supply the electric field E to the specimen crystal, a pair of electrodes, as shown in Figure 2 was used: a specimen about $5 \times 5 \times 0.1$ mm^3 in dimension with the largest surface parallel to (001) was prepared from a flux-grown butterfly twin crystal, and was sandwiched between copper electrodes to apply the field in the direction parallel to [001]. An X-ray beam slit 1×5 mm^2 in size was used at the front electrode.

3 RESULTS

At first, the intensity distribution of the 400 peak was measured with S1 fully open and S2 0.05 mm in width. The scan steps of ω and 2θ were 0.025 and 0.06 mrad, respectively. The counting time at each step was 30 s, and the peak intensity was about 100 cps. In Figure 3, the intensity contour maps in the $\omega - 2\theta$ space are shown at 418 K, 17 K above the transition temperature T_c: (a) for $E = 0$, and (b) for $E = 0.87$ kV/mm. The effect of the electric field on the intensity distribution is remarkable but mostly limited in the ω direction: the full-width at half-maximum (FWHM) in ω are 0.8 and 0.3 mrad in (a) and (b) respectively, while that in 2θ is 0.5 mrad for both cases. Then, by ω scanning, measurements of the rocking curve were made as a function of E, at 428 K. As shown in Figure 4, FWHM linearly decreases with increasing E, reaches 0.3 mrad at 0.6 kV/mm, and remains at higher fields; this behaviour is reversible and reproducible as a function of E.

On the other hand, a rocking curve with FWHM 0.3 mrad was also observed even at $E = 0$ by narrowing S1 to less than 0.4 mm. This indicates that the specimen crystal consists of grains, and that the dispersion of crystallographic axes of grains may roughly

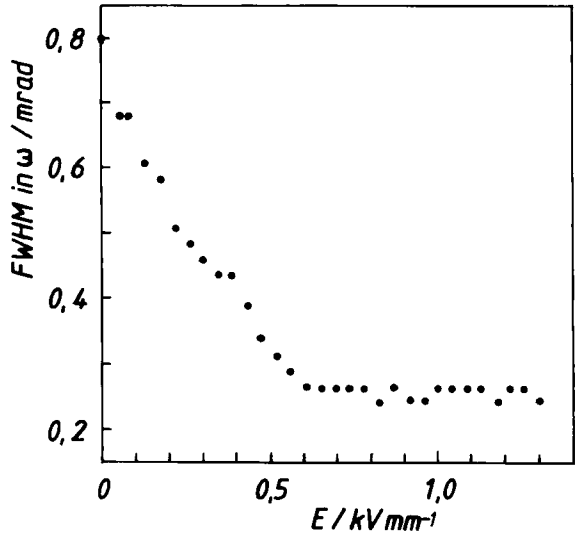

Figure 4 FWHM in ω at 428 K as a function of E.

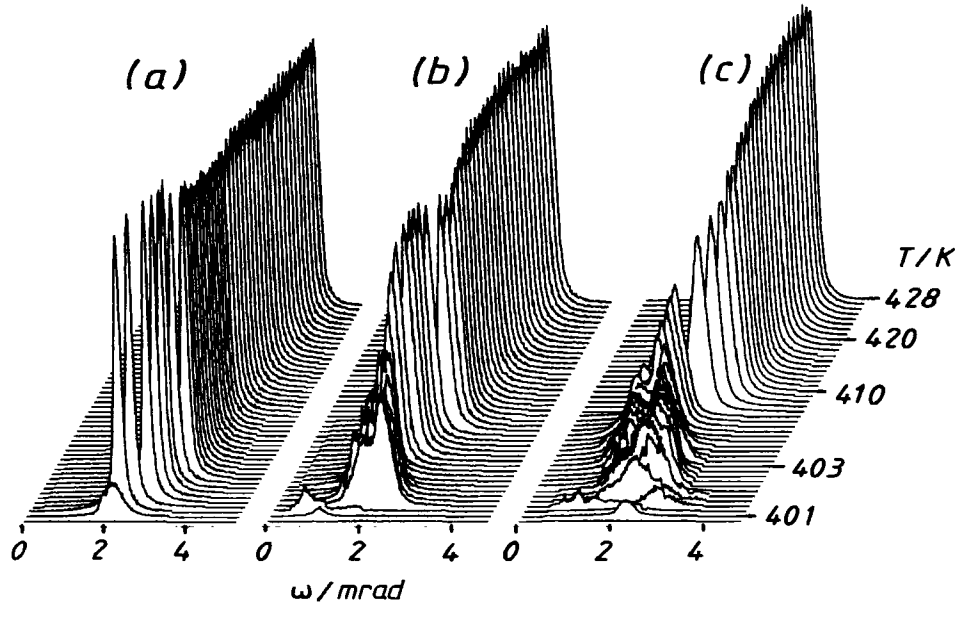

Figure 5 400 diffraction profiles as a function of temperature: (a) in E=0, (b) in E=0.87, and (c) in E=1.74 kV/mm.

be 0.3 mrad. According to these features, the behaviour of the FWHM shown in Figure 4 can readily be explained: though the orientation of grains is dispersed within 0.8 msterad at $E = 0$, better alignment is attained by applying the external field with a saturation at $E \geq 0.6$ kV/mm. In order to confirm the effect of E on the intrinsic crystallographic properties, and not on the grain alignment, further measurements were made on a single grain by limiting the region of examination on the specimen surface with S1 0.5×0.4 mm^2 in size: FWHM in ω of the observed rocking curve was 0.3 mrad at $E = 0$. Rocking curves were observed as a function of temperature; the electric field was varied in the range 0–1.74 kV/mm at intervals of 0.218 kV/mm. In Figures 5(a), (b) and (c), the profiles observed on cooling at $E = 0$, 0.87 and 1.74 kV/mm are shown respectively as examples; in (a), no remarkable change in the profile was observed down to a temperature close to the transition, where the peak of the cubic phase vanishes. In (b) and (c), in contrast, the peak begins to broaden at higher temperatures, and collapses near the transition.

4 DISCUSSION

For a quantitative discussion of the peak broadening shown in Figure 5, the peak height, integrated intensity and FWHM have been analysed; the results are shown in Figures 6(a), (b) and (c), respectively, as functions of temperature and field. The lines in the figure are guides for the eye. If we ignore the behaviour in the region just above the transition, where the integrated intensity is so weak that a quantitative discussion is not allowed, the results can be summarised as follows. Firstly, except for when $E = 0$, an increase in the FWHM and a decrease in the peak height are observed with decreasing temperature, while the integrated intensity is kept constant. This means that, during the process of peak broadening, the volume of the cubic phase does not vary. In other words, no second phase appears above T_C. Secondly, the broadening starts at higher temperatures in stronger fields. In Figure 7, the initial temperature T_B for broadening is plotted as a function of E. In the figure, the relations between the Curie temperature and applied field given by Merz (1953) are also shown by two lines: the solid and broken lines, respectively, indicate the relations determined from hysteresis loop experiments and from a calculation based on the theory by Devonshire (1949). From this figure, it is clear that the Curie temperature (T_C) given by Merz corresponds to the broadening temperature observed in the present work. Therefore, we conclude that the lines indicate T_B, not T_C, as a function of E. A kind of ferroelectricity appears below T_B, but the cubic symmetry remains.

Although the crystal structure in the temperature range of interest is not known yet, the eight-site disordered model by Itoh *et al.* (1985) is consistent with the present result; the ferroelectric cubic state can be explained by assuming that a part of the eight sites vanishes as a kind of critical fluctuation induced by the external field. Moreover, the model is suitable for grain rearrangement in the field: the model structure may have sensitivity in the external electric field.

Full details of the peak broadening described here will be made clearer in a future high-resolution X-ray diffraction study by means of the 2θ-resolved HADOX: the peak broadening in ω and 2θ will be specified by analysing the two-dimensional intensity distribution, and this will enable us to discuss the crystal and/or grain structures in the cubic phase.

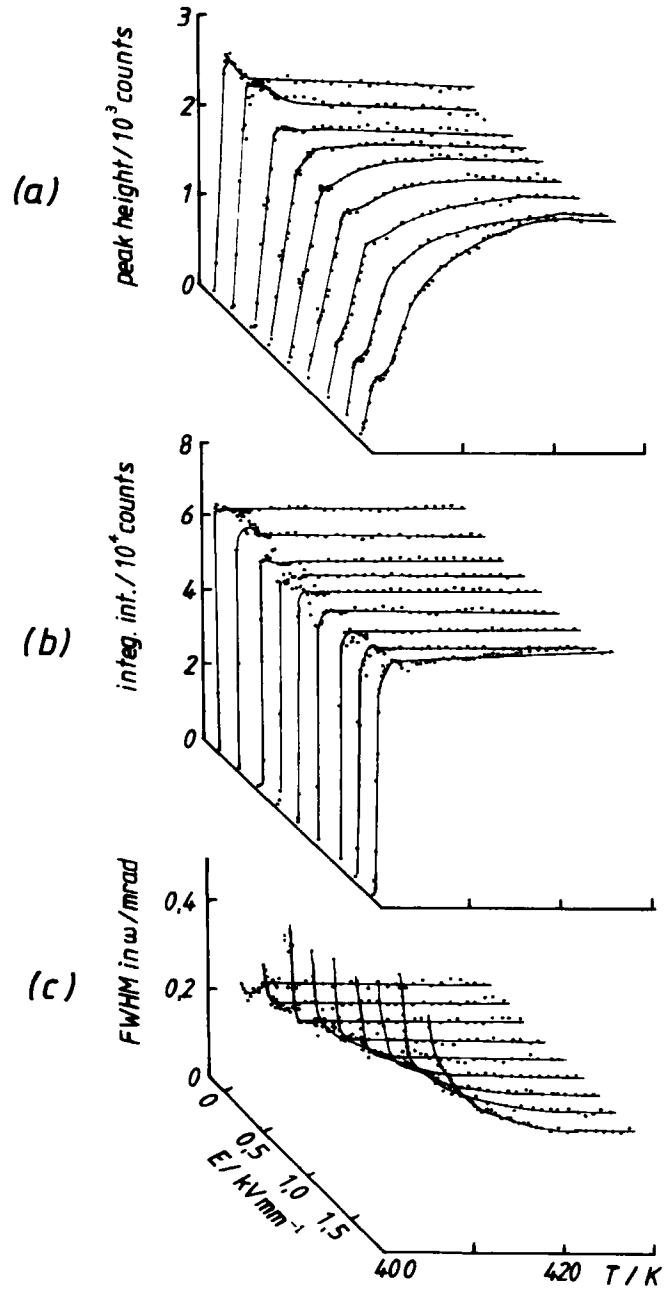

Figure 6 Temperature and field dependences of (a) peak height, (b) integrated intensity, and (c) FWHM in ω.

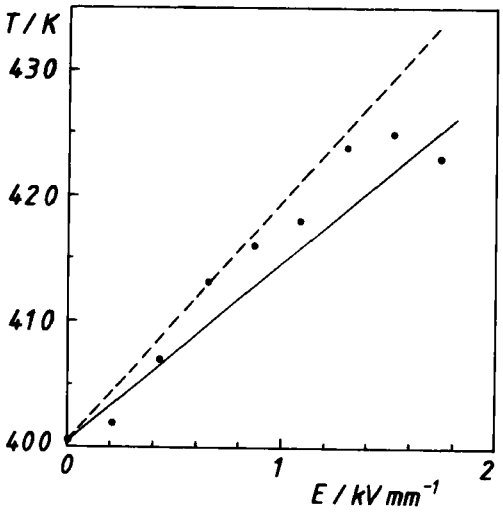

Figure 7 Plot of broadening temperature T_B vs. E. Solid and broken lines are described in the text.

Acknowledgements

The authors are grateful to Professor A. Okazaki and Dr. Z. Lu for discussions and comments.

References

Comes, R., M. Lambert and A. Guinier (1968). The chain structure of $BaTiO_3$ and $KNbO_3$. *Solid State Commun.*, **6**, 715–719.

Devonshire, A.F. (1949). Theory of barium titanate – Part I. *Phil. Mag.*, **40**, 1040–1063.

Dougherty, T.P., G.P. Wiederrecht and K.A. Nelson (1994). Femtosecond time-resolved spectroscopy of soft modes in structural phase transitions of perovskites. *Phys. Rev.*, **B50**, 8996–9019.

Inoue, K. (1983). Study of structural phase transitions by the hyper-Raman scattering. *Ferroelectrics*, **52**, 253–262.

Inoue, K. and S. Akimoto (1983). Hyper-Raman scattering spectra in the low frequency range in cubic $BaTiO_3$ and the mechanism of the phase transition. *Solid State Commun.*, **46**, 441–445.

Itoh, K., L.Z. Zeng, E. Nakamura and N. Mishima (1985). Crystal structure of $BaTiO_3$ in the cubic phase. *Ferroelectrics*, **63**, 29–37.

Merz, W.J. (1953). Double hysteresis loop of $BaTiO_3$ at the Curie point. *Phys. Rev.*, **91**, 513–517.

Ohama, N., H. Sakasita and A. Okazaki (1979). Improvement of high-angle double-crystal X-ray diffractometry (HADOX) for measuring temperature dependence of lattice constants. II. Practice. *J. Appl. Cryst.*, **12**, 455–459.

Okazaki, A. and N. Ohama (1979). Improvement of high-angle double-crystal X-ray diffractometry (HADOX) for measuring temperature dependence of lattice constants. I. Theory. *J. Appl. Cryst.*, **12**, 450–454.

Onitsuka, H., M. Hatakeyama, Y. Soejima and A. Okazaki (1994). A 2θ-resolved HADOX study of $BaTiO_3$ Linz crystals. *Phase Transitions*, **47**, 93–103.

Soejima, Y., N. Tomonaga, H. Onitsuka and A. Okazaki (1991). Two-dimensional intensity distribution in high-angle double-crystal X-ray diffratometry (HADOX). *Z. Kristallogr.*, **195**, 161–168.

Takahashi, H. (1961). A note on the theory of barium titanate. *J. Phys. Soc. Jpn.*, **16**, 1685–1689.

Tomonaga, N., Y. Soejima and A. Okazaki (1990). A 2θ-resolved HADOX study of $BaTiO_3$. *Phase Transitions*, **28**, 51–61.